The use of ANN and conventional solar-plant meteorological variables to estimate atmospheric horizontal extinction

J. Alonso-Montesinos[a,b,*], J. Ballestrín[c], G. López[d], E. Carra[c], J. Polo[e], A. Marzo[f], J. Barbero[a], F. J. Batlles[a,b]

[a] *Department of Chemistry and Physics, University of Almería, 04120 Almería, Spain.*
[b] *CIESOL, Joint Centre of the University of Almería-CIEMAT, 04120 Almería, Spain.*
[c] *Concentrating Solar System Unit (Plataforma Solar de Almería, CIEMAT), 04200 Almería, Spain.*
[d] *Department of Electrical and Thermal Engineering, Design and Projects, University of Huelva, 21004 Huelva, Spain.*
[e] *Photovoltaic Solar Energy Unity (Renewable Energy Division-CIEMAT, 28040 Madrid, Spain*
[f] *CDEA, University of Antofagasta, 02800 Antofagasta, Chile*

Abstract

In the search to optimize electricity generation systems based on renewable energy sources, solar power plants are a clear alternative for reducing pollution on the planet. In particular, concentrating solar power plants with central tower technology supply energy to large population centers and they are generally located at desert sites. Production in these plants drops due to the presence of particles in the environment. These particles are complex to measure and doing so usually requires the use of dedicated, expensive

*Corresponding author: Telephone: +34 950 214430
Email address: joaquin.alonso@ual.es (J. Alonso-Montesinos)

instrumentation. In this work, we present a methodology called Extinction that estimates this attenuation phenomenon utilizing meteorological variables, along with the use of artificial neural networks (ANN). Direct normal irradiance, relative humidity, temperature and pressure have been the only meteorological variables needed to estimate the Extinction. The results from the estimations presented a correlation coefficient value (R) of 0.88 (between the measured and estimated atmospheric horizontal extinction with ANN), a normalized Mean Bias Error (nMBE) of 0% and a normalized Root-Mean Square Deviation (nRMSD) of 7%.
Keywords: Atmospheric Extinction; solar energy; image processing; CSP plants; PV plants; ANN

1. Introduction

To reduce the impact of greenhouse gases in the atmosphere Yang et al. (2020), conventional systems of electricity production are seeing their potential reduced; this is thanks to the emergence of other cleaner systems based on renewable energies Bamisile et al. (2020). Renewables are energy sources that fundamentally originate from the sun. Because of this, they create continual challenges in terms of optimization and discovering valid opportunities for generating electricity Guelpa et al. (2019).

Solar energy is one of the most widely used sources for producing electricity because of the potential of the sun's resource, especially in the Earth's sunbelt. The sun, as an unlimited and constant source, provides sufficient energy to be able to produce electricity and meet the demand, whether residential or industrial in nature.

Central solar tower power (CSTP) plants have experienced an increase in installed electrical potential over the last decade Ávila Marín (2011); this is because of the high efficiency achieved in systems with thermal storage, fundamentally in molten salts, allowing production to take place uninterruptedly during the day and night (Mostafavi Tehrani et al. (2018).

CSTP plants require direct normal irradiance (DNI) as an energy source to reflect and concentrate the energy potential onto the focal point at the top of the tower, where the receiver is located. Along this optical path, from the solar field mirrors (called heliostats) to the receiver sitting on the tower, there are losses caused by the appearance of suspended particles, such as aerosols Sengupta and Wagner (2011), dust particles Ferrada et al. (2019) or water vapor in the lower layers of the atmosphere Gueymard et al. (2017b). In the past, this was generally ignored when designing and starting up these plants Polo et al. (2018); however, it was later discovered that in desert locations,

drops in performance led to major losses in final system production Alonso-Montesinos et al. (2019), especially during extreme dust episodes Gueymard et al. (2017a), as in the case of Almería (southern Spain) Alonso-Montesinos et al. (2017) and in the Arabic Sea (India) Aswini et al. (2020). Similarly, in photovoltaic (PV) plants, the need to link atmospheric extinction with dust deposition is highlighted as one of the most important factors causing production losses Trigo-Gonzalez et al. (2019).

Several techniques are used to calculate the losses produced between the concentration system and the tower's focal point, based on measured or estimated extinction values in the lower layers of the atmosphere; these, for example, are considered in radiative transference models Polo et al. (2016). To this end, several works have been carried out using different methodologies. Other authors used two different commercial instruments at the Plataforma Solar de Almería(PSA) - the Vaisala FS11 scatometer, which provides a monochromatic near-infrared light source emission and measures the strength of scattering processes in a small air volume caused mainly by aerosol particles, and the Optec LPV4 long-path visibility transmissometer, which determines the monochromatic attenuation between a light emitting diode (LED) light source at 532 nm. Both instruments were used to deter-

mine the meteorological optical range (MOR) Hanrieder et al. (2015). The authors modelled 1 km extinction ramps from the heliostats to the central tower's receiver. Following on from this work, the DNI-based transmittance model was combined with the Beer-Lambert law to determine transmittance using the Root Mean Square Error (RMSE), which was between 5 and 9% (Hanrieder et al. 2019). Recently, a system based on two digital cameras has been employed, which focused on the same Lambertian target, but at different distances Ballestrín et al. (2016). This development has provided a novel method for determining atmospheric extinction at the PSA by comparing images captured at the same time using both cameras. In addition, campaigns have been carried out to compare the average extinction rates at the PSA site, obtaining an average annual extinction coefficient of 0.081 km^{-1} Ballestrín et al. (2019).

Clearly, there is great interest in knowing the losses produced along the CSTP's heliostat-plant receptor path. The tasks of optimizing CSTP plant operation help to improve control services related to electricity production by ensuring clean systems, contributing to an improved environment, thus reducing the earth system's carbon footprint.

In this work, the typical meteorological variables of a solar plant (DNI,

relative humidity, ambient air temperature, pressure and wind speed) have been used to develop an artificial intelligence system, based on Artificial Neural Networks (ANN), where the variable to be estimated is the atmospheric horizontal extinction in the CSTP plants. This provides a novel method that does not require specific instrumentation, and can therefore be implemented anywhere that the above-mentioned variables are available. With this new methodology, which optimizes solar applications that do not emit carbon into the atmosphere, solar thermal plants can better manage the energy produced in their plants, knowing (in-situ) the energy losses that might arise during solar concentration and that might affect the plant's energy use.

2. Materials and methods

In this section, a detailed description is given of the processes carried out using ANN to estimate the atmospheric extinction at the Plataforma Solar de Almería. Further sections will present the PSA's characteristics, the system for determining the atmospheric extinction and the ANN properties for modeling the input variables.

2.1. Plataforma Solar de Almería

The Plataforma Solar de Almería is a research, development and testing center dedicated to concentrating solar technology. The PSA is located in the Tabernas desert in the southeast of Spain ($37^o05´$ north and $2^o21´$ west); it has a semi-arid climate, close to a dry Mediterranean climate. The site receives more than 1900 $kWh.m^{-2}.year^{-1}$ in annual solar radiation, an average annual irradiance of 517 Wm^{-2} and a maximum irradiance of 1045 Wm^{-2}.

The PSA site is ideal for a solar power plant, with more than 3000 sun hours a year. Furthermore, its personnel have more than 30 years of experience in operating, maintaining and evaluating solar concentration systems. Currently, the PSA has a wide variety of experimental facilities and R&D laboratories for activities related to solar thermal concentration systems.

2.2. Extinction measurement using two digital cameras

For the present work, atmospheric extinction has been measured using a measurement system developed at the PSA Ballestrín et al. (2018). The system consists of two identical optical systems based on digital cameras ((Hamamatsu, model ORCA-flash4.0 v3 Complementary Metal Oxide Semiconductor (CMOS)) using suitable lenses and filters, each having a spectral range of 400 to 1000 nm. To measure solar atmospheric extinction, the se-

lected cameras have a 16 bit A/D conversion output, which makes the cameras dynamical range 0-65535 (216-1), the effective number of pixels 2048(H) x 2048(V), the cell size 6.5 µm x 6.5 µm, the quantum efficiency higher than 82% at 600 nm and 60% at 750 nm, and an exposure time of 1 ms to 10 s Ballestrín et al. (2018).

The cameras are located on the north-south line of the PSA, at different distances from the target. The target has a Lambertian surface with dimensions of 2 x 2 m. Figure 1 shows a schema of the camera and target configuration.

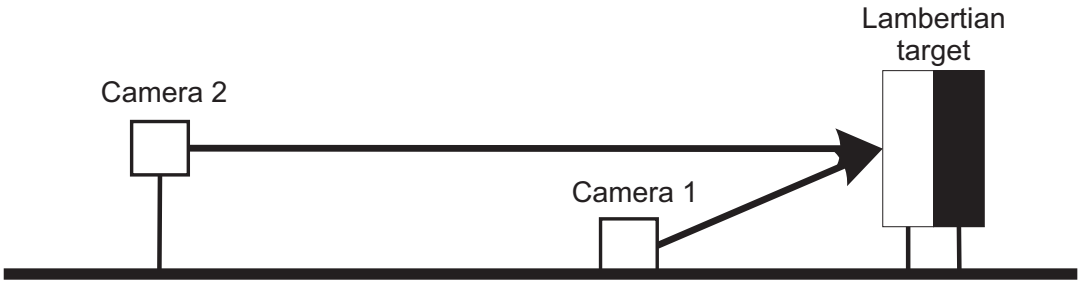

Figure 1: Configuration of cameras and Lambertian target in the PSA emplacement for the Extinction measurement.

The measurement procedure consists of simultaneous target imaging by both cameras using two identical optical systems (comprising the digital camera's sensor, lens and filter). The cameras detect radiation from an area of interest on the target, the intensity levels obtained from both cameras' images being proportional to the amount of radiation from the target. Using

these intensity levels and a simple algorithm Ballestrín et al. (2018), the atmospheric horizontal extinction for the distance between the cameras is obtained, with an absolute measurement uncertainty of less than 2%. The attenuation is determined by comparing the two images, following Eq. 1:

$$Extinction\ (\%) = 100\left(1 - \frac{I_2}{I_1}\right), \tag{1}$$

where I_1 (I_1=I_{1W}-I_{1B}) and I_2 (I_2=I_{2W}-I_{2B}) are the average intensities of the images, I_{1W} represents the average intensities from the white target of camera 1, I_{1B} represents the average intensities from the black target of camera 1, I_{2W} represents the average intensities from the white target of camera 2 and I_{2B} represents the average intensities from the black target of camera 2.

Almost three years of extinction measurements have been gathered and the system continues to operate with only minimum maintenance required Ballestrín et al. (2018).

All the measurements have been filtered daily, eliminating a small amount of them (<5%) due to camera saturation effects caused by unwanted solar radiation reflections from the clouds on the Lambertian target. Moreover, meteorological value errors were removed from the database to guarantee

correct atmospheric horizontal extinction modelling.

2.3. Artificial Neural Networks

Increasingly, advances in computational systems endeavor to represent human actions. ANNs are tools inspired by the neurological functioning of the human brain, where a set of input signals activate several functions to obtain a final result. The relationship between the inputs and the final variables is defined by past actions; therefore, it is necessary to have many experiences to model the behavior of the input dataset. The modeling process, known as training, defines the patterns in which the relationships are defined, creating a set of hidden layers that receive the entry pattern already modified by the relevant activation functions, sharing the results of this processing with all the neurons in the next layer by means of new activation functions. Finally, the result is obtained in the last neuron layer. Figure 2 shows a general representation of this process.

Therefore, the first step consists of determining the input dataset according to the variables used for modeling a desired output.

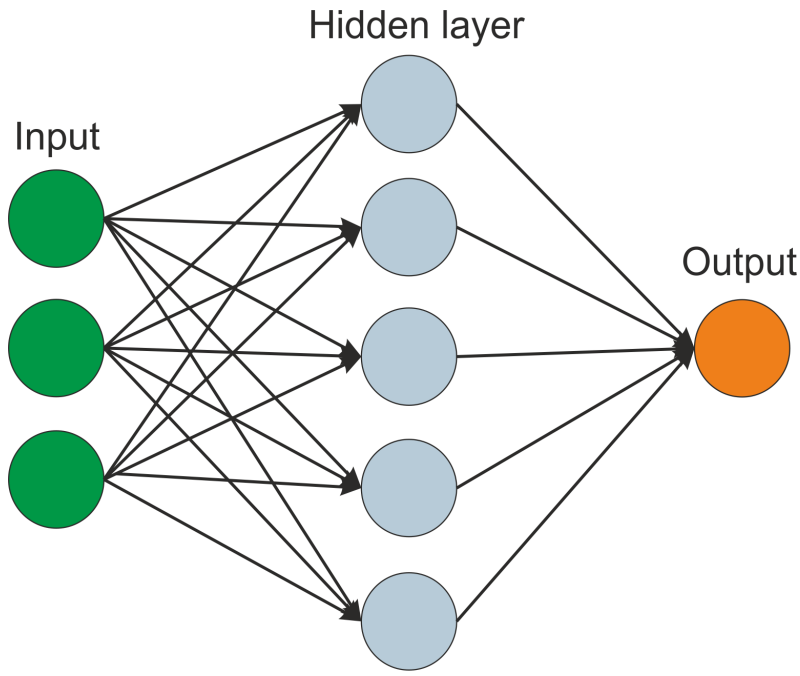

Figure 2: General schema of artificial neural networks.

2.4. Analysis of the relevance of variables

In a first approach, one should determine which variables have more influence in the extinction modeling . For this, a total of five commonly measured variables from a CSP plant were used: DNI (Wm^{-2}), Relative Humidity (RH) (%), atmospheric Pressure (P) (mb), ambient air Temperature (T) (^oC) and Wind Speed (WS) (km h^{-1}). Each measured variable was correlated with the extinction measurements to establish the degree of concordance prior to the ANN modeling. The correlation is quantified through the correlation coefficient (R) (Eq. 2), which is used to determine the agreement between an

input dataset and the output; thus, a value near ±1 indicates good agreement (positive or negative) and a 0 value determines that no correlation exists.

$$R = \frac{\sigma_{Extinction_{est}Extinction_{mea}}}{\sigma_{Extinction_{est}}\sigma_{Extinction_{mea}}}, \tag{2}$$

where $\sigma_{Extinction_{est}Extinction_{mea}}$ is the covariance of the two input data sets (the estimated extinction obtained from the ANN model and the measured extinction), $\sigma_{Extinction_{est}}$ is the standard Extinction$_{est}$ deviation and $\sigma_{Extinction_{mea}}$ is the standard Extinction$_{mea}$ deviation.

Fig. 3 shows a graphical representation of each variable against the extinction, where the correlation coefficient (R) appears in each sub-graph.

According to the five graphs represented in Figure 3, the best correlations are given by ambient temperature and atmospheric pressure, with R values of 0.59 and -0.50, respectively. The negative sign of R is consistent. This is a consequence and not a cause of extinction, but the ANN does not care about that. If cloudiness had been eliminated, the value of R would have been higher. In the case of T and P, it has also sensed that the R coefficients have a different sign. Curiously, the RH shows a near 0 correlation with the extinction, which supposes a non-correlation between the two compared variables, similar to that of wind speed. However, there are studies in

which the RH showed a strong relationship with the extinction López et al. (2018). Therefore, the R coefficient for the RH is especially influential in lineal situations with extinction; however, extinction is not usually lineal under normal conditions. In general terms, probably the poorest variable for representing the extinction is wind speed (R=0.01), where the influence of wind directionality makes wind speed ambiguous and confusing as a variable.

2.5. Determining the set of variables for the ANN

Next, to consider the relevance of each variable with respect to extinction, one of the most important actions when configuring an ANN is to choose the best combination of input variables. Initially, all the available variables are introduced into the ANN to see if it is possible to delete some of them; if so, this improves the statistical results and reduces the computational costs. In this step, using the ANN results, one can contrast the variables' primary relevance analyses. Together with the R coefficient, the Mean Square Error (MSE) (Eq. 3) has also been used to determine the difference between the estimations and the real measurements.

$$MSE = \frac{1}{N}\sum_{i=1}^{N}(Extinction_{est} - Extinction_{mea})^2 \tag{3}$$

where N is the total number of cases; Extinction_{est} is the estimated extinction and Extinction_{mea} is the measured extinction.

With these two statistical indicators (R and MSE), the best input combination is selected as the best input vector. This process is part of the neural network training, in which three different stages are identified: training, validation and testing. In this work, a total of 18405 data registers were collected over the period from 28th June 2017 to 12th March 2019, in which all the variables were filtered to ensure quality and synchronism. Each dataset was registered every 15 minutes, avoiding moments with low solar altitude (according to the CSTP plant's operation timing). From the totality of cases, 80% of the random cases (14724 cases) were used to train the ANN whereas 20% (3681 cases) were used for the validation stage. However, to ensure good representation and fit of the random sets, a normal distribution was configured in the selection process. Figure 4 shows the distribution of random cases for the 80% data set.

Figure 4 shows a representation of the data selected as the ANN training set in the form of a histogram and a fit line. The overlapping histograms represent the data volume for each extinction band with two different scales while the fitting curve is centered on the histogram with the largest ampli-

tudes. In it, one can surmise that the largest data volume is collected for Ext values between 4% and 5%, comprising around 4500 cases.

For the validation process, 20% of the data (independent from the training data) are used to validate the ANN model. Figure 5 shows the normal distribution for the 20% of selected process validation data.

Looking at Figure 5, one can see a distribution and trends that are very similar to those for the training data set, which suggests that both the training and validation data sets follow a homogeneous and equitable data distribution.

Once the datasets for the neural network are defined, an iterative process is needed to determine the best set of variables for determining the atmospheric extinction. The idea is to compare different combinations to find the one with the smallest error.

When an ANN is created in the Matlab environment, one must set the different properties such as the percentage of data for training, validation and testing. In this case, we determined 20% of data as independent. As with the 20% of independent data collected in Fig. 5 (above), the aim was to use the remaining 80% for training purposes (Fig. 4). However, in spite of wanting to use the full 80% of data for training, in Matlab it is mandatory to reserve

a minimal percentage for validating and testing the training process. In this case, 5% was allocated for each process. In other words, from the 80% of data destined for training, 90% are used for training the neural network while the rest are used for testing and validating the training process. Numerically, this means a total of 13252 registers for training, 736 for validation and 736 for testing. For network matching, 10 hidden neurons were defined and the Levenberg-Marquardt training algorithm was used for all cases due to its robustness and rapid convergence Motahar and Bagheri-Esfeh (2020). Table 1 presents the combinations carried out to determine the best ANN model, where the statistical indices indicate the corresponding information to quantify the accuracy of the ANN for the training (train.), validation (valid.) and testing (test.) processes, together with the number of iterations (Iter.) for choosing the optimal cycles (Cycles). The results are obtained next to one execution of the ANN in Matlab environment.

One can see that in ANN 1, the R Training is 0.83. This is then used as the optimal starting correlation. Already, ANN 2 has eliminated one variable, and this happens again with the rest of the networks up to ANN 6 (networks with only 4 variables). The best combination is that which determines the highest correlation, and this happens when WS is eliminated.

Table 1: Representation of the statistical errors for the different combinations of the input variables in the ANN modeling.

ANN name	DNI	RH	T	P	WS	MSE train.	R train	MSE valid.	R valid	MSE test.	R test	Cycles	Iter.
ANN 1	x	x	x	x	x	1.74	0.83	1.82	0.83	1.53	0.85	17	23
ANN 2	x	x	x	x		1.49	0.85	1.41	0.85	1.37	0.87	54	60
ANN 3	x	x	x		x	2.01	0.79	1.99	0.81	2.03	0.79	55	61
ANN 4	x	x		x	x	1.98	0.80	1.87	0.79	1.77	0.81	35	41
ANN 5	x		x	x	x	1.81	0.82	1.76	0.81	0.85	0.82	30	36
ANN 6		x	x	x	x	1.91	0.81	2.08	0.80	1.77	0.82	60	66
ANN 7	x	x	x			2.12	0.78	2.03	0.78	1.96	0.77	73	79
ANN 8	x	x		x		2.19	0.77	2.03	0.77	2.09	0.80	15	21
ANN 9	x		x	x		1.96	0.80	1.76	0.81	1.99	0.81	21	27
ANN 10		x	x	x		2.23	0.77	2.07	0.78	2.30	0.76	6	12

It even improves with 5 variables (with respect to ANN 1) demonstrating that WS is a noisy network parameter – firstly because it provides no information and secondly because it generates worse correlations. Regarding WS, the wind directionality would be necessary to make sense of the speed since it could indicate if the wind is coming from an area where it can drag in particles and suspend them in the air. Therefore, after observing the R Training value of ANN 2 - 6, the best correlation is ANN 2 with an R value of 0.85. Following this determination, we move to a new cycle, in which new input vectors are combined, removing the WS variable (ANN 7 to 10). Accordingly, we observe that none of the defined networks improve the ANN 2 results, and therefore we can determine that ANN 2 is the best network.

The subsequent step is to study whether it is possible to improve this

network by increasing the number of hidden neurons. Remember that we started with a similar situation for all cases, 10 hidden neurons; from now on, we will gradually increase the number until we find the best correlation. Table 2 shows the statistical errors for ANN 2, determined by varying the number of hidden neurons (HN).

Table 2: Representation of the statistical errors for the ANN 2 varying the number of hidden neurons.

ANN name	DNI	RH	T	P	HN	MSE train.	R train	MSE valid.	R valid	MSE test.	R test	Cycles	Iter.
ANN 2_2	x	x	x	x	20	1.27	0.88	1.06	0.90	1.16	0.88	109	115
ANN 2_3	x	x	x	x	30	1.03	0.90	0.99	0.90	0.97	0.91	156	162

Observing the table (Table 1) for determining the definitive ANN (with 20 hidden neurons), we can see it is ANN 2_2 that presents an improvement over ANN 2, obtaining an R Training value of 0.88. We then increase the ANN by another 10 neurons, obtaining ANN 2_3; in this case, we again improve the correlation slightly, going to 0.90. However, the number of cycles and iterations make the network a little more expensive in terms of time. Therefore, to achieve greater network efficiency, and given the fairly similar results, ANN 2_2 is selected as the best network for determining the extinction, using only DNI, HR, P and T. Figure 6 shows the graphs obtained in the training process to obtain the optimal number of iterations (109).

In this figure, one can see how, from iteration 109 onwards, the MSE remains practically linear; thus, a training cut-off point is required so as not to expand the time and operations any further. Figure 7 shows the histogram with the data set used for training, validation and testing, where Ext_{mea} is the measured extinction and Ext_{est} is the estimated extinction obtained using ANN 2_2.

One can also observe that the highest number of cases is found for situations where there is no error (the Zero Error line), with the histogram similar to the Gaussian bell curve; this shows that the ANN model concentrates the highest number of cases in situations with zero error. Finally, Figure 8 presents the scatter plots for the ANN Training, Validation and Testing results.

The scatter plots show the trends in the data used for the ANN. The abscissa axes represent the extinction measurement values while the ordinate axes represent the values determined by the ANN. In almost all cases, the Ext value is below 15%, highlighting the lineal trends in all the processes.

Therefore, by carrying out these tasks, an ANN is created that determines the extinction values for the PSA using common meteorological variables. In the next section, the results of this work are presented, where certain statis-

tical indices have been used, such as the Mean Bias Error (MBE) and the Root-Mean Square Deviation (RMSD), as absolute and percentage values. In addition, the correlation coefficient (R) has also been determined. Equations 4-7 show the definitions of each index.

$$nMBE(\%of error) = 100\frac{MBE}{Ext_{max} - Ext_{min}}, \tag{4}$$

where the MBE is calculated using Eq. 5, with Ext_{max} being the maximum extinction value measured and Ext_{min} being the lowest extinction value measured.

$$MBE(\%of Extinction) = \frac{1}{N}\sum_{i=1}^{N}(Ext_{est} - Ext_{mea}) \tag{5}$$

For the RMSD, Eq. 6 defines the mathematical function.

$$nRMSD(\%of error) = 100\frac{RMSD}{Ext_{max} - Ext_{min}}, \tag{6}$$

where RMSD is calculated using Eq. 7:

$$RMSD(\%\ of\ Extinction) = \sqrt{\frac{1}{N}\sum_{i=1}^{N}(Ext_{est} - Ext_{mea})^2} \tag{7}$$

3. Results

In this section, we present the results of the work, in which a neural network has been defined for estimating the atmospheric horizontal extinction using the four meteorological variables. The results are given in a general way, depending on the extinction ranges.

3.1. General results

Once the network has been defined, it remains to be tested with the 20% of situations (3681 cases) that are totally independent from those of the training (Fig. 5). To do this, a routine was created in MATLAB that allows one to run ANN 2_2 with an external dataset. After running the routine, the extinction was estimated. Figure 9 represents a scatter plot between the measured and the estimated extinction using ANN.

In this graph, one can see that the dispersion trend is quite good, following an almost perfect line, with the highest concentration of points on the main diagonal, maintaining a very marked and good trend. To appreciate this trend more clearly, Figure 10 shows a graphical representation of the estimated and measured extinction values against the number of cases.

One can see how the two curves present a very close evolution, perfectly

attending to the trend of the real data. Therefore, this is quite a precise estimation model. Furthermore, it only requires meteorological variables that are commonly measured in any central tower solar thermal plant.

Table 3 shows the statistical indices obtained after evaluating the ANN model (ANN 2_2) against the real extinction values.

Table 3: Statistical indices for the evaluation of the Extinction estimation with ANN.

ANN name	MBE	nMBE	RMSD	nRMSD	R
ANN 2_2	0.00	0.08	1.13	7.06	0.88

If we look at the values for the MBE and the nMBE, it tells us that, in general, the model has practically no overestimation or underestimation, with very well compensated results at the global level. If we study the RMSD value, we see that there is an average of 1.13% extinction, while the normalized values are approximately 7%, indicating a good relationship between the estimated and measured values, as also indicated by the R coefficient, which has a similar value to that of the training.

3.2. Results classified by extinction levels

Given that the number of cases analyzed in the validation data set was not homogeneous for all the extinction values, three different groups have

been defined, each with varying extinction ranges. Table 4 shows the results of the statistical indices for each data subset.

Table 4: Statistical indices for the evaluation of the Extinction estimation with ANN, according to Extinction ranges.

ANN name	Extinction range (%)	Cases	MBE	nMBE	RMSD	nRMSD	R
ANN 2_2	[0,4[	1347	-0.59	-15.42	1.19	31.2	0.38
ANN 2_2	[4,8[	1851	0.25	6.24	1.06	26.41	0.72
ANN 2_2	$\geq$8	483	0.71	8.73	1.24	15.11	0.54

In this table, one can see that most of the data have values between 4 and 8% extinction, according to the Gaussian center of the normal distribution (Fig. 5). As for the results, it should be noted that, for extinction values lower than 4%, the ANN is usually underestimated, with values close to 15%, while in the rest of the cases, the tendency is to overestimate the extinction (always below 9%). As for the nRMSD, the best results were for situations with high extinction values, above 8%, while the correlation coefficient determined that the best correlations were for the set with more data, with a value higher than 0.70.

To appreciate these results in graphic form, different graphs were created. Figure 11 shows the results of the extinction estimation together with the measured values for the situations in which the extinction was lower than

4%.

In this graph, one can see how the ANN presents practically the same trends, always following the same patterns of extinction measurements, but usually overestimating the values (already seen in Fig. 9). For these data, the MBE was negative. The next classification is for extinction values between 4 and 8%. Figure 12 shows the trends.

This graph shows that very similar patterns are followed for the data set studied. It should be noted that the bulk of the data is found in this strip; therefore the ANN has learned more, and there is greater proximity between the measured and the estimated Ext values. In this case, the R coefficient presented a value of 0.72. Finally, Figure 13 presents the graphic results of the extinction estimations together with the real values for situations where the extinction was higher than 8%.

It is clear that very similar trends are shown in most of the situations studied, with the ANN defining the sequence pattern very effectively, which (as indicated) captures and represents the variations of extinction over time with great certainty and synchronism.

4. Conclusions and discussion

This paper presents a methodology for developing an artificial neural network to estimate atmospheric horizontal extinction in CSTP plants using common meteorological variables that are available in any solar technology installation.

To develop the network, the initial data set was divided for training and validation processes according to the percentages indicated in the corresponding section. The most optimal input data set was defined as being DNI, RH, T and P, while WS was eliminated because it created noise in the network and led to worse results. The neural network results were compared against a system based on two local digital cameras that measured extinction, developed at the Plataforma Solar de Almería.

The statistical indices showed an R value of 0.88 and an average MSE of 1.27% for the training phase, using the training data. The resulting ANN was developed with 20 hidden neurons (which provided more efficient results than when using a greater number of hidden neurons) containing 109 cycles. In the validation process, which used the validation data, the results showed an nMBE of the order of 0%, while the nRMSD presented a value close to 7% with an R value that coincided with the training process.

In the work carried out in Ballestrín et al. (2018), the authors created a novel system to determine the horizontal atmospheric extinction, based on two digital cameras, positioned at different distances from a Lambertian surface. The results obtained were an nRMSD of 7% and an R value of 0.93, with an underestimation of the values of 2.3%, according to the nMBD value. The horizontal atmospheric extinction was also determined using the relative humidity value and the value returned by a particle counter of 0.25 - 32 mum Ballestrín et al. (2020). In this work, the value of the two variables was introduced in an NNA to estimate the atmospheric extinction, where in nRMSD was less than 6% and the R value of 0.92, having for this a total of 184 measurements between 3 and 21 July 2018. As can be seen, the work presented in this article, presents very similar results, with the interest of not using the camera system or a particle counter, making it more widespread and adaptable to other locations.

The results were also grouped by extinction values between 0 and 4 percent, between 4 and 8 percent and over 8 percent. In the case of values below 4%, the ANN underestimated the extinction value, presenting an nMBE value of around 15% and an RMSD value slightly above 1%. In the intermediate group of extinction values, a slight overestimation in the extinction values

was shown, with an MBE of 0.25% and an RMSD value of approximately 1%. In addition, since there were more cases in this extinction range, the R value was 0.72. When the extinction was greater than 8%, the MBE value was below 1% of extinction, and presented the lowest nRMSD of close to 15%.

Analyzing the advantages of this work, it is necessary to highlight the interest aroused by the CSTP plants, to know in real time the power losses in the central receptor of the plant, caused by suspended particles that generate atmospheric horizontal extinction. It can be included in any study evaluating losses, such as for quantifying the drop in irradiance between the heliostats and the central receiver of a CSP plant, or for gauging dust deposition on photovoltaic panels due to suspended dust phenomena in photovoltaic plants, which can be related to high extinction rates. Moreover, in a monitored system, it would be possible to include this application to quantify the effective irradiance and, therefore, the production of a solar-origin power system. Also, extreme dust events are difficult to model, creating uncertainty about their effects on plant production, so far not quantified in a sophisticated way. Therefore, having knowledge of atmospheric horizontal extinction serves to determine operating strategies for a plant, as well as to

more accurately model a CSTP plant prior to its creation. However, until now, specific and expensive instrumentation was required, not always available in this type of plants. It is difficult to control dust episodes, due to their characteristics and distribution. Furthermore, atmospheric extinction is a local variable and, therefore, depends on the meteorology and climatology of the place, making it difficult to extrapolate methodologies with traditional techniques and linear correlations.

To sum up, this work offers an accurate and efficient system for determining atmospheric horizontal extinction in solar plants. The importance of this work lies in estimating an atmospheric horizontal extinction coefficient, determined with variables commonly measured in a solar plant. It is very important to emphasize that the results have shown that the extinction can be modeled with a very good approximation, using meteorological variables that are simple to measure, and without needing to make important financial investments for sophisticated measurement systems.

As future lines of research, it will be possible to find new supervised learning techniques, including self-learning, with the emergence of new scenarios, which will further maximize the accuracy of the extinction estimation. In addition, the inclusion of other meteorological solar plant variables could

be considered, whenever they are available, as well as solar geometry parameters. There is also a desire to model the system with other commonly available parameters, without the need for sophisticated instruments such as scatometers, digital cameras or particle counters, like in this work.

5. Acknowledgements

The author would like to thank the PRESOL Project (references ENE2014-59454-C3-1, 2 and 3) and the PVCastSOIL Project (references ENE2017-83790-C3-1, 2 and 3), which were funded by the *Ministerio de Economía, Industria y Competitividad* and co-financed by the *European Regional Development Fund*. We would also like to acknowledge the financial support provided by Chilean Economic Development Agency (CORFO) contract No 17BPE3-83761.

References

Alonso-Montesinos, J., Barbero, J., Polo, J., López, G., Ballestrín, J., Batlles, F., 2017. Impact of a saharan dust intrusion over southern spain on dni estimation with sky cameras. Atmospheric Environment 170, 279–289.

Alonso-Montesinos, J., Monterreal, R., Fernández-Reche, J., Ballestrín, J.,

Carra, E., Polo, J., Barbero, J., Batlles, F., López, G., Enrique, R., Martínez-Durbán, M., Marzo, A., 2019. Intra-hour energy potential forecasting in a central solar power plant receiver combining Meteosat images and atmospheric extinction. Energy 188.

Aswini, M., Kumar, A., Das, S., 2020. Quantification of long-range transported aeolian dust towards the Indian peninsular region using satellite and ground-based data - A case study during a dust storm over the Arabian Sea. Atmospheric Research 239.

Ballestrín, J., Carra, E., Alonso-Montesinos, J., López, G., Polo, J., Marzo, A., Fernández-Reche, J., Barbero, J., Batlles, F., 2020. Modeling solar extinction using artificial neural networks. Application to solar tower plants. Energy 199.

Ballestrín, J., Carra, E., Monterreal, R., Enrique, R., Polo, J., Fernández-Reche, J., Barbero, J., Marzo, A., Alonso-Montesinos, J., López, G., Batlles, F., 2019. One year of solar extinction measurements at Plataforma Solar de Almería. Application to solar tower plants. Renewable Energy 136, 1002 – 1011.

Ballestrín, J., Monterreal, R., Carra, M.E., Fernández-Reche, J., Barbero,

J., Marzo, A., 2016. Measurement of solar extinction in tower plants with digital cameras. AIP Conference Proceedings 1734, 130002.

Ballestrín, J., Monterreal, R., Carra, M.E., Fernández-Reche, J., Polo, J., Enrique, R., Marzo, A., 2018. Solar extinction measurement system based on digital cameras. Application to solar power tower plants. Renewable Energy 125, 648–654.

Bamisile, O., Huang, Q., Xu, X., Hu, W., Liu, W., Liu, Z., Chen, Z., 2020. An approach for sustainable energy planning towards 100% electrification of Nigeria by 2030. Energy 197.

Ferrada, P., Olivares, D., del Campo, V., Marzo, A., Araya, F., Cabrera, E., Llanos, J., Correa-Puerta, J., Portillo, C., Román Silva, D., Trigo-Gonzalez, M., Alonso-Montesinos, J., López, G., Polo, J., Batlles, F., Fuentealba, E., 2019. Physicochemical characterization of soiling from photovoltaic facilities in arid locations in the atacama desert. Solar Energy 187, 47–56.

Guelpa, E., Bischi, A., Verda, V., Chertkov, M., Lund, H., 2019. Towards future infrastructures for sustainable multi-energy systems: A review. Energy 184, 2–21.

Gueymard, C., Al-Rasheedi, M., Ismail, A., Hussain, T., 2017a. Long-term variability of aerosol optical depth, dust episodes, and direct normal irradiance over Kuwait for CSP applications. ISES Solar World Congress 2017 - IEA SHC International Conference on Solar Heating and Cooling for Buildings and Industry 2017, Proceedings , 75–84.

Gueymard, C.A., López, G., Rapp-Arrarás, I., 2017b. Atmospheric transmission loss in mirror-to-tower slant ranges due to water vapor. AIP Conference Proceedings 1850, 140010.

Hanrieder, N., Wilbert, S., Pitz-Paal, R., Emde, C., Gasteiger, J., Mayer, B., Polo, J., 2015. Atmospheric extinction in solar tower plants: absorption and broadband correction for mor measurements. Atmospheric Measurement Techniques 8, 3467–3480.

López, G., Gueymard, C., Bosch, J., Rapp-Arrarás, I., Alonso-Montesinos, J., Pulido-Calvo, I., Ballestrín, J., Polo, J., Barbero, J., 2018. Modeling water vapor impacts on the solar irradiance reaching the receiver of a solar tower plant by means of artificial neural networks. Solar Energy 169, 34–39.

Ávila Marín, A., 2011. Volumetric receivers in Solar Thermal Power Plants

with Central Receiver System technology: A review. Solar Energy 85, 891–910.

Mostafavi Tehrani, S., Shoraka, Y., Nithyanandam, K., Taylor, R., 2018. Cyclic performance of cascaded and multi-layered solid-PCM shell-and-tube thermal energy storage systems: A case study of the 19.9 MWe Gemasolar CSP plant. Applied Energy 228, 240–253.

Motahar, S., Bagheri-Esfeh, H., 2020. Artificial neural network based assessment of grid-connected photovoltaic thermal systems in heating dominated regions of Iran. Sustainable Energy Technologies and Assessments 39, 100694.

Polo, J., Alonso-Montesinos, J., López-Rodriguez, G., Ballestrín, J., Bosch, J., Barbero, J., Carra, E., Fernández-Reche, J., Batlles, F., 2018. Modelling atmospheric attenuation at different AOD time-scales in yield performance of solar tower plants. AIP Conference Proceedings 2033.

Polo, J., Ballestrín, J., Carra, E., 2016. Sensitivity study for modelling atmospheric attenuation of solar radiation with radiative transfer models and the impact in solar tower plant production. Solar Energy 134, 219–227.

Sengupta, M., Wagner, M.J., 2011. Impact of aerosols on atmospheric attenuation loss in central receiver systems: Preprint.

Trigo-Gonzalez, M., Batlles, F., Alonso-Montesinos, J., Ferrada, P., del Sagrado, J., Martínez-Durbán, M., Cortés, M., Portillo, C., Marzo, A., 2019. Hourly pv production estimation by means of an exportable multiple linear regression model. Renewable Energy 135, 303–312.

Yang, Z., Wang, B., Jiao, K., 2020. Life cycle assessment of fuel cell, electric and internal combustion engine vehicles under different fuel scenarios and driving mileages in China. Energy 198.

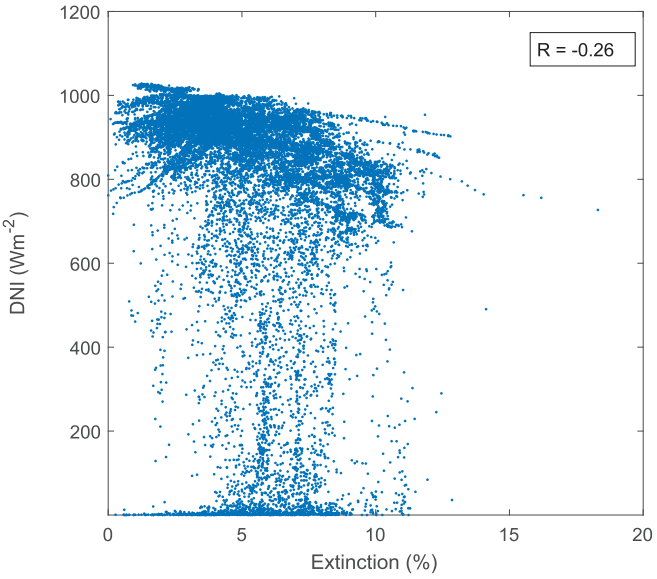
R = -0.26
DNI (Wm-2)
Extinction (%)

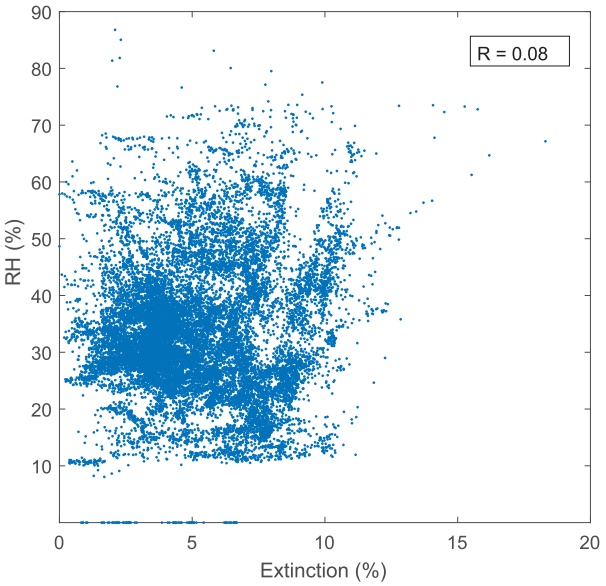
R = 0.08
RH (%)
Extinction (%)

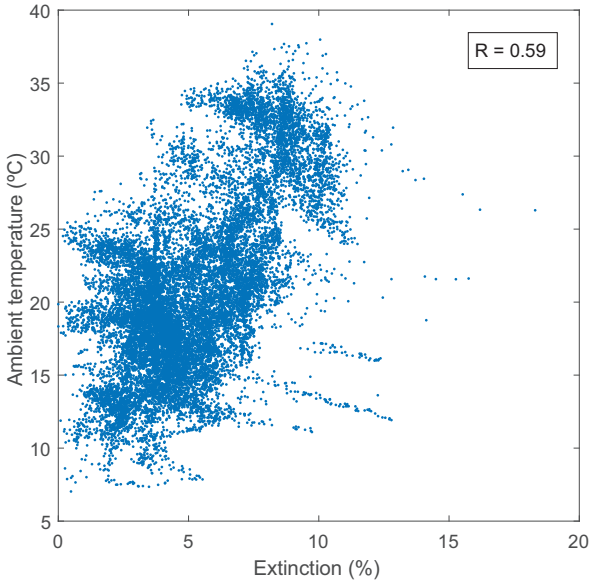
R = 0.59
Ambient temperature (ºC)
Extinction (%)

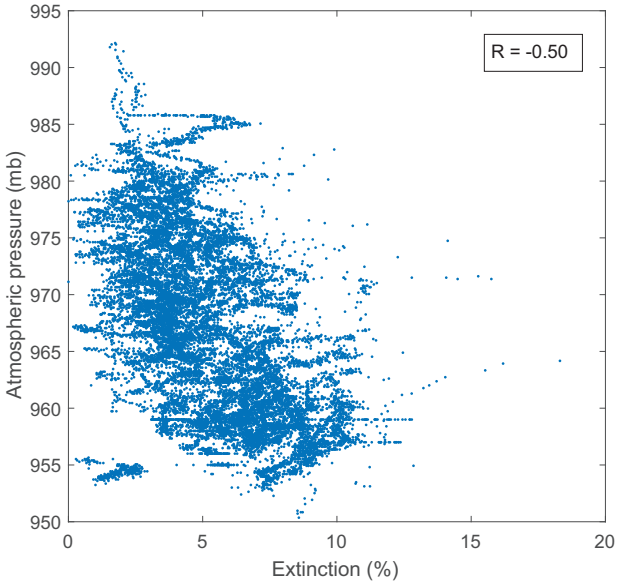
R = -0.50
Atmospheric pressure (mb)
Extinction (%)

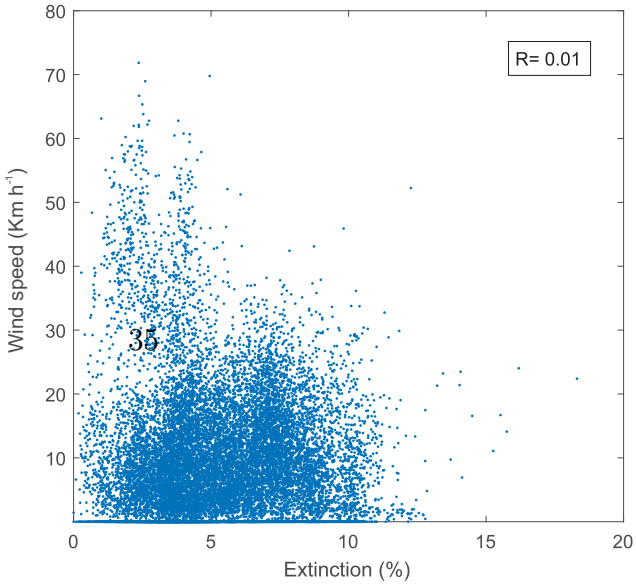
R= 0.01
Wind speed (Km h-1)
Extinction (%)

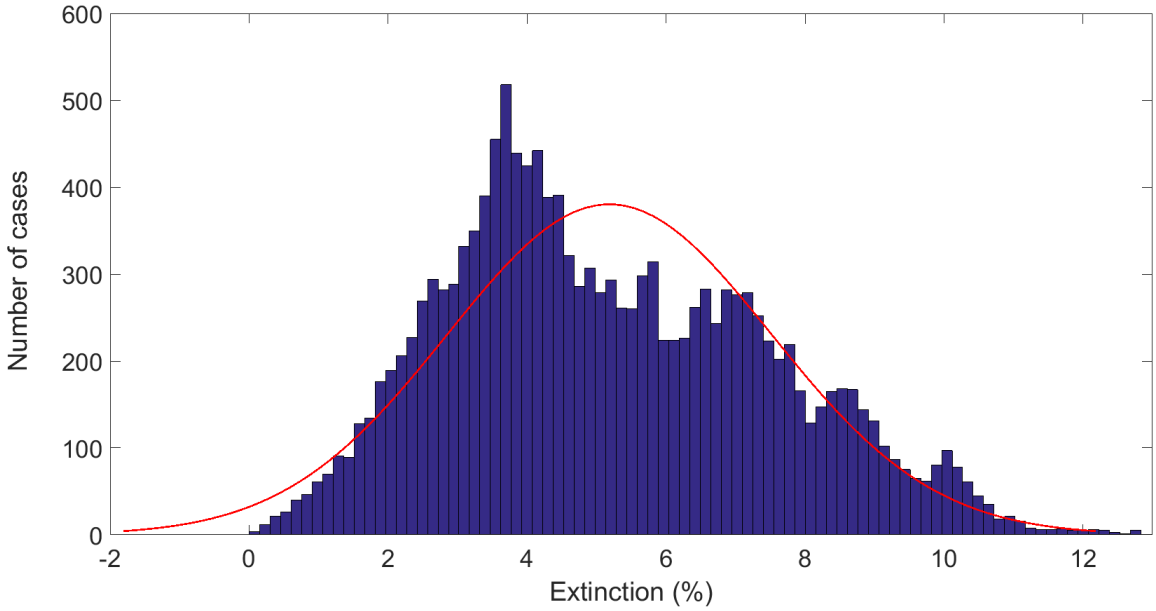

Figure 4: Normal distribution with the 80% of the random data for the ANN training process.

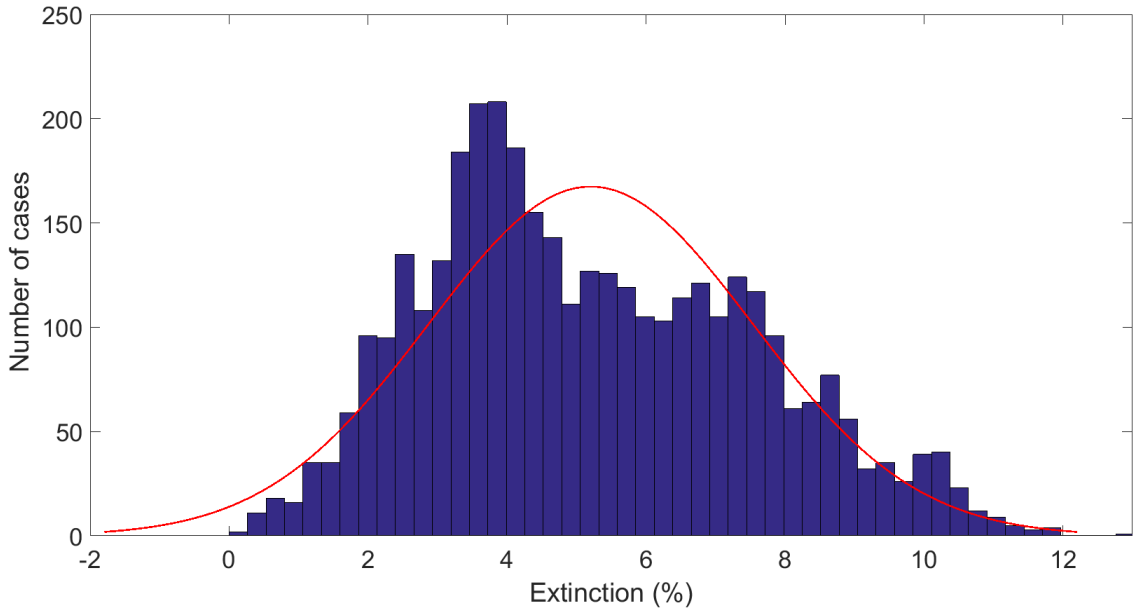

Figure 5: Normal distribution of the 20% data for the ANN validation process.

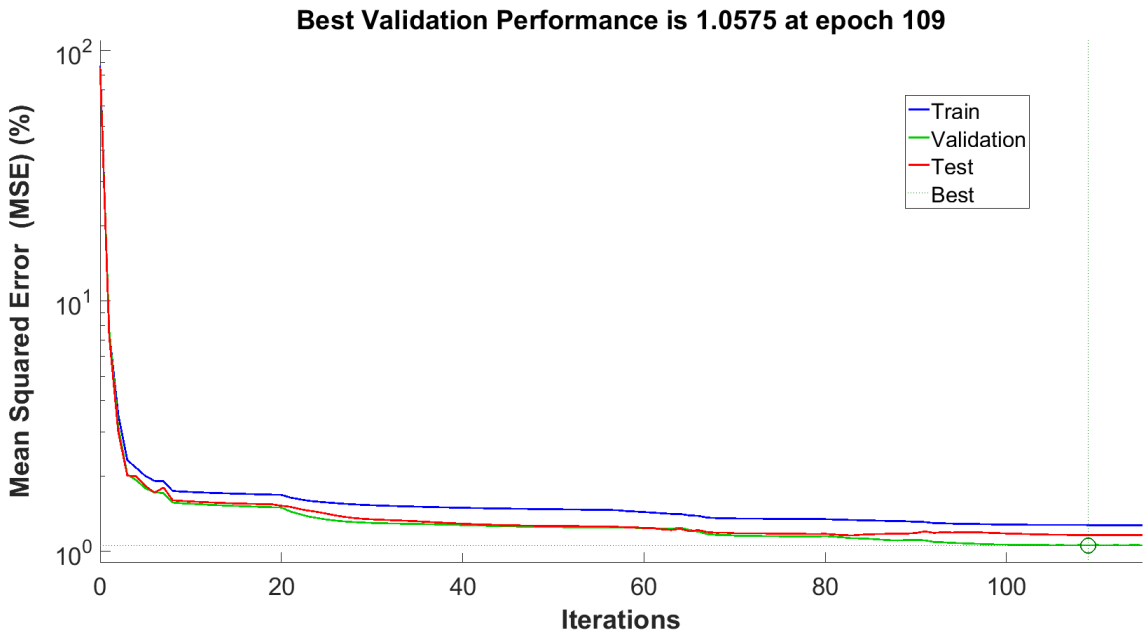

Figure 6: Graphical vision to obtain the optimal number of cycles in the training of the neural network ANN 2_2.

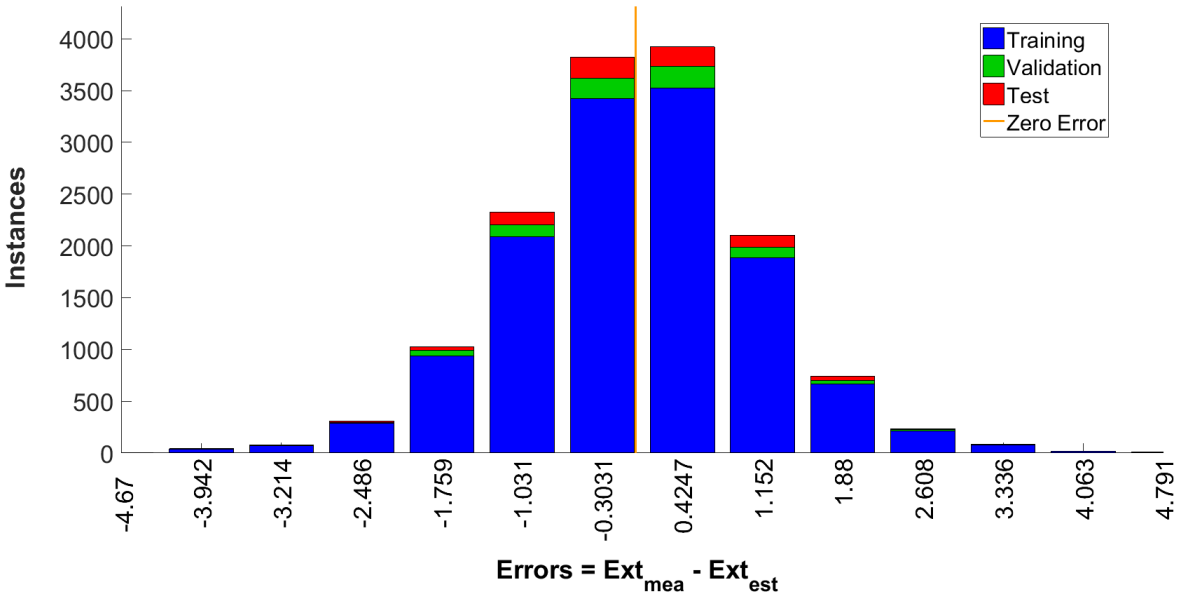

Figure 7: Error Histogram graph for the neural network ANN 2_2.

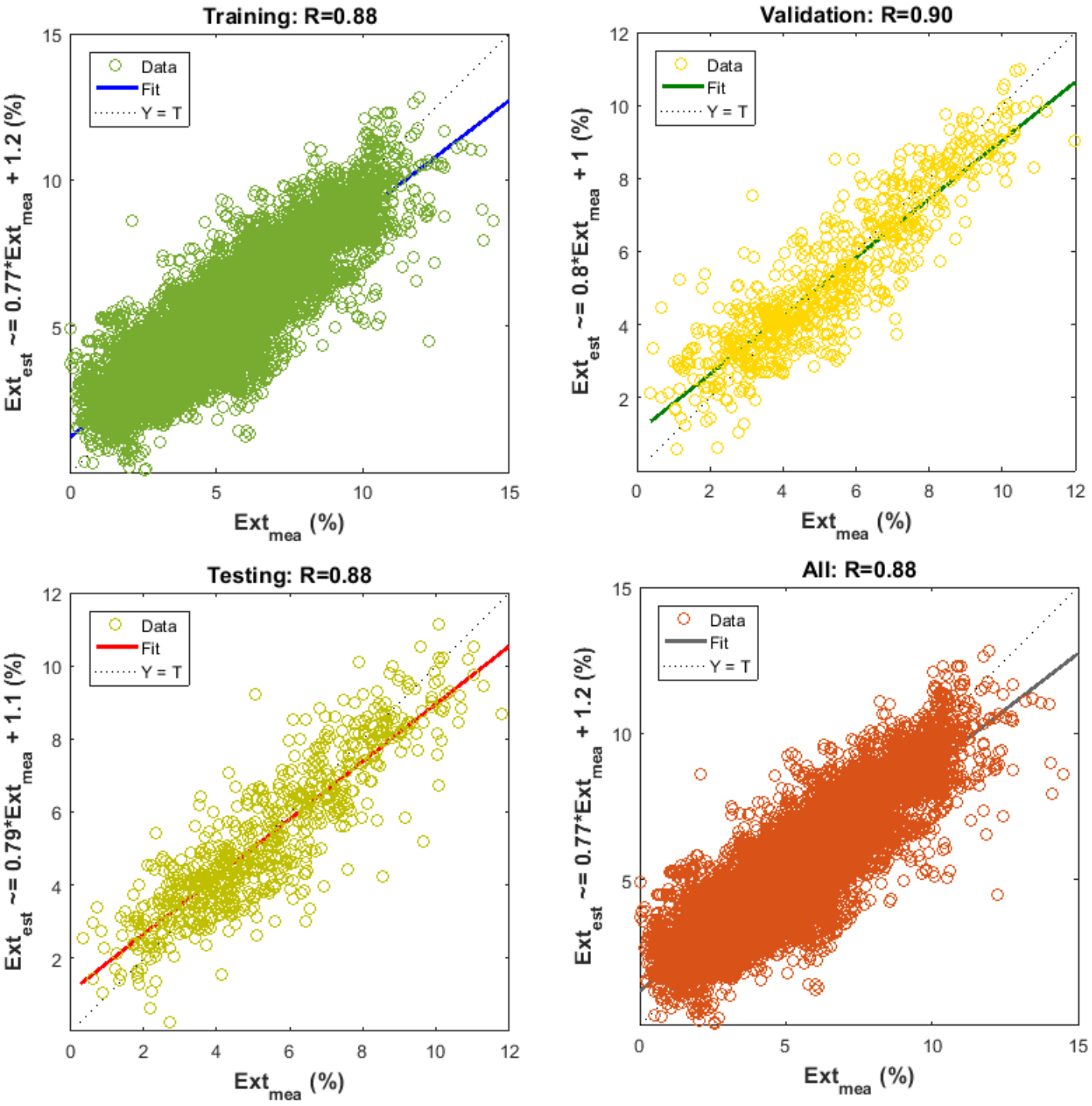

Figure 8: Scatter diagrams with the results of the processes carried out for the ANN 2_2 modeling.

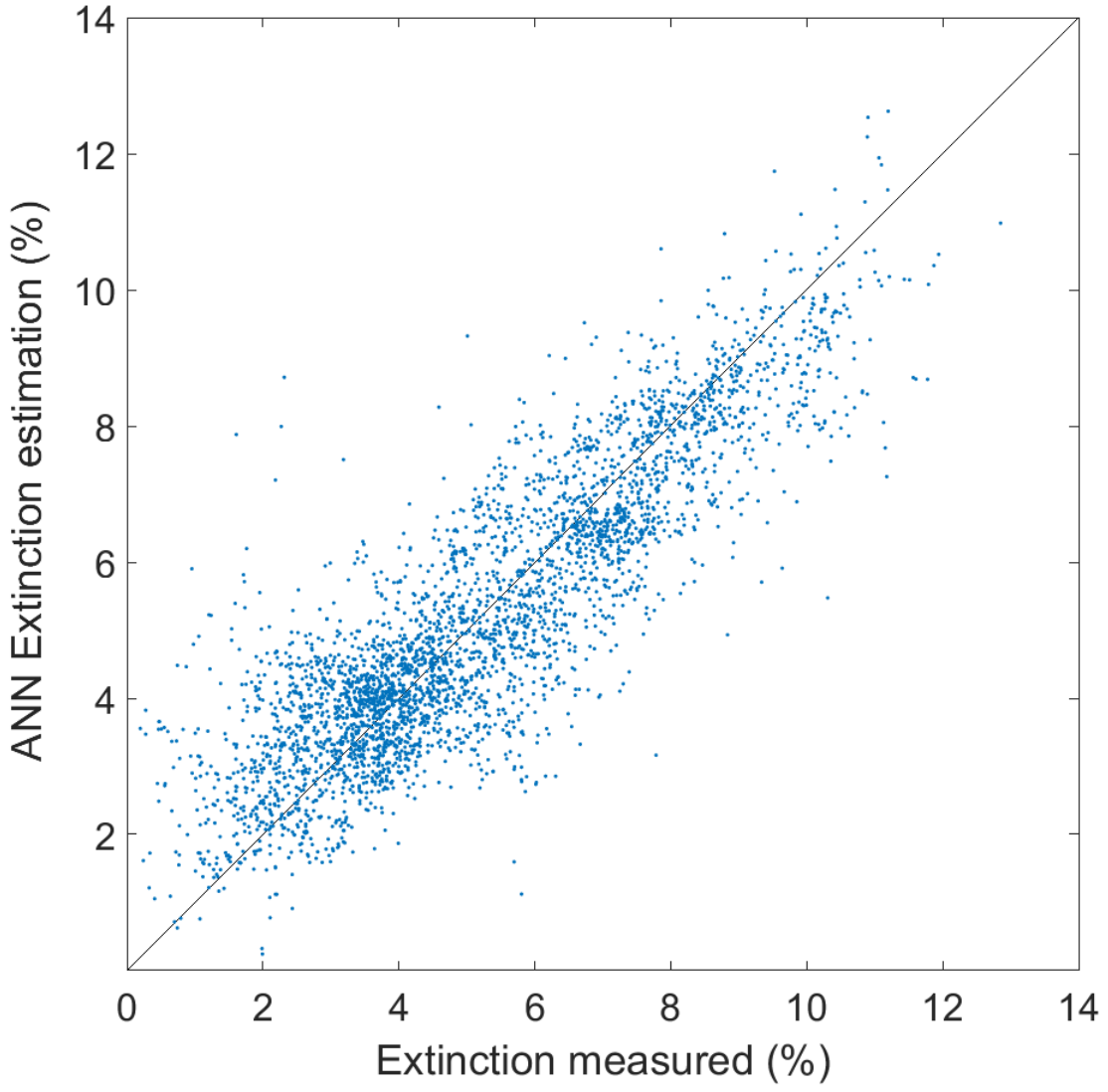

Figure 9: Scatter plot with the independent data set for testing and analyzing the ANN 2_2.

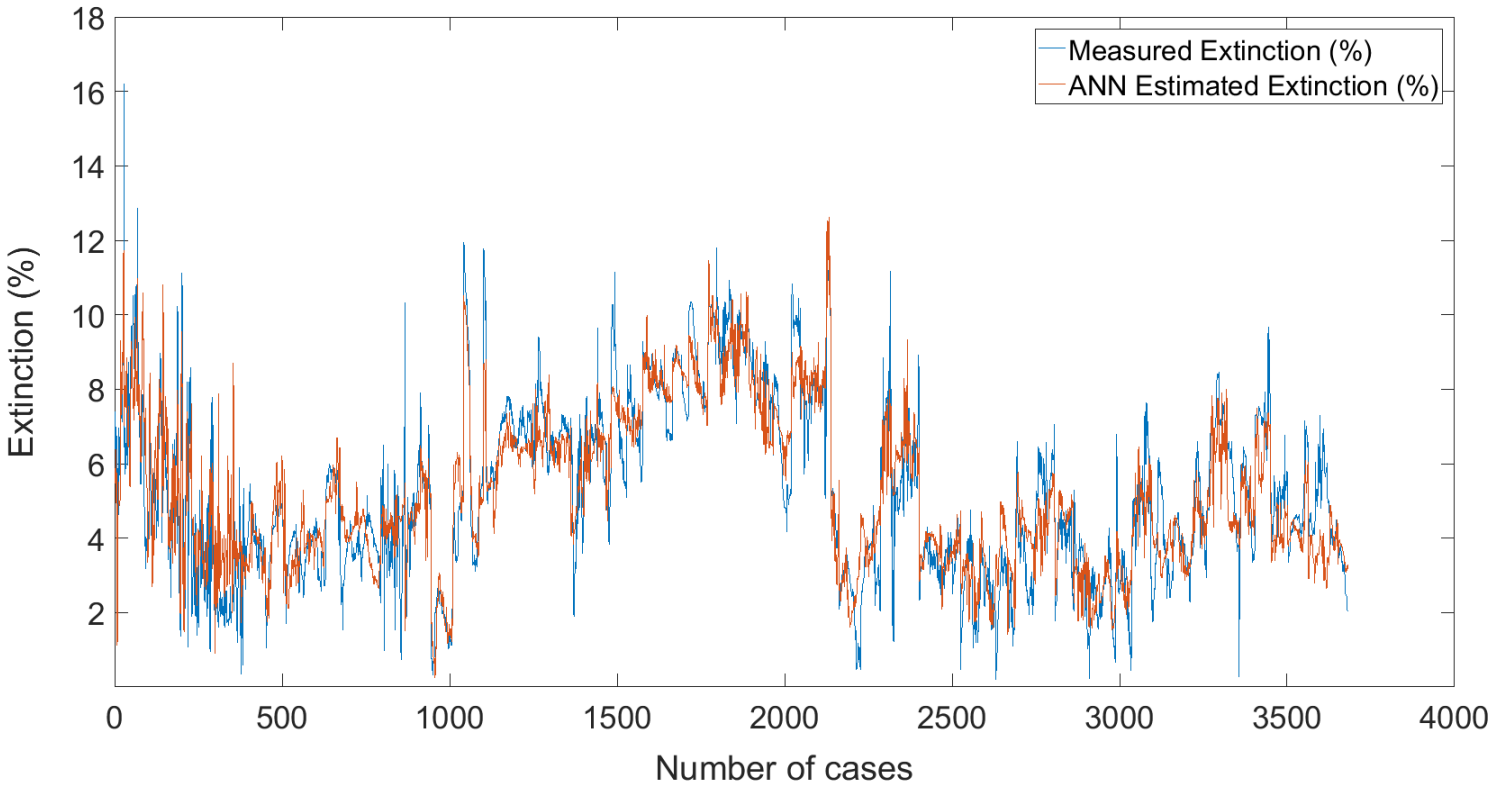

Figure 10: Graph with the independent validation data set, where the measured and estimated Extinction with the neural network are displayed.

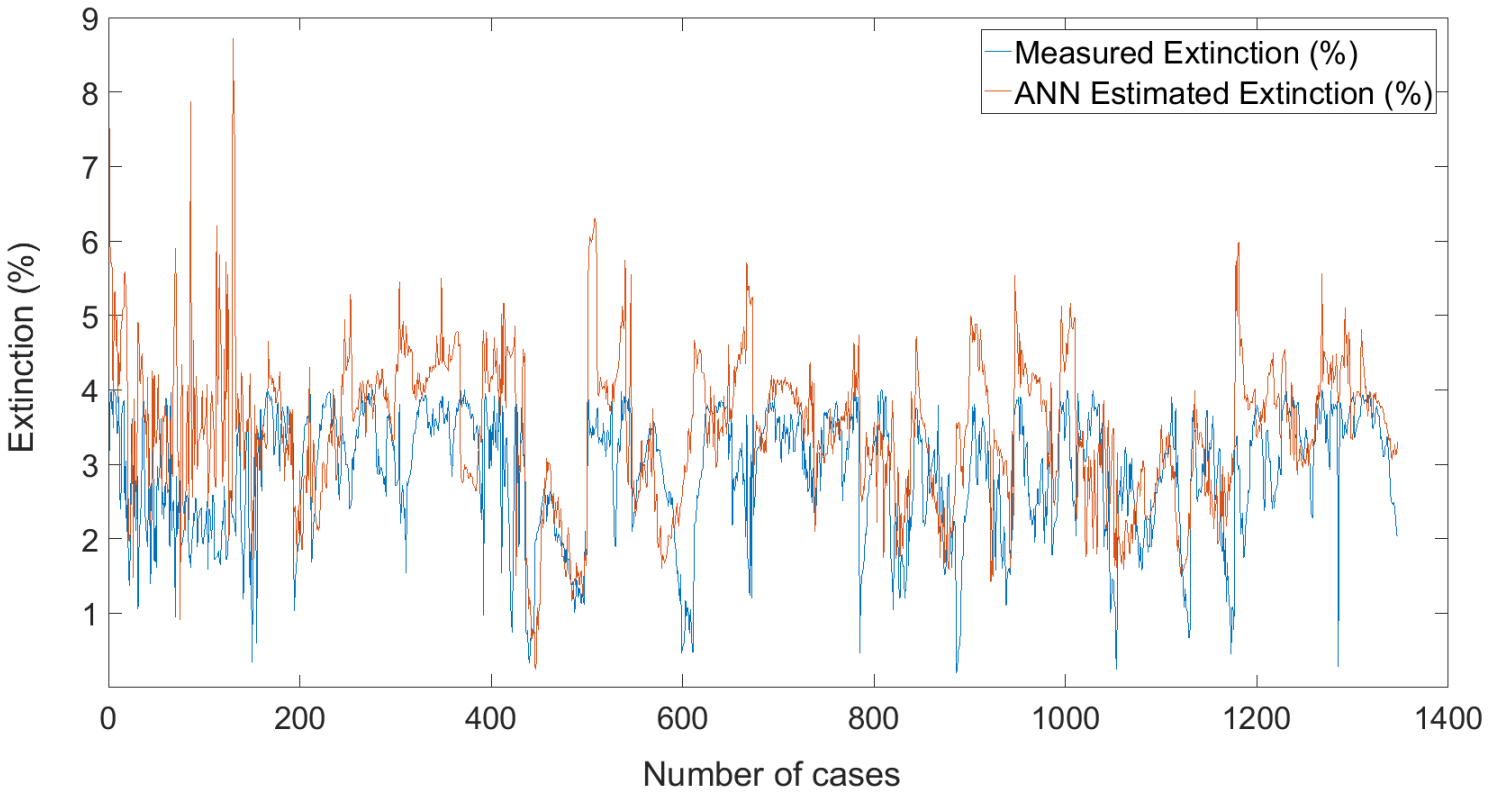

Figure 11: Scatter plot with the independent data set for testing and analyzing the ANN 2_2, where the Extinction is lower than 4%.

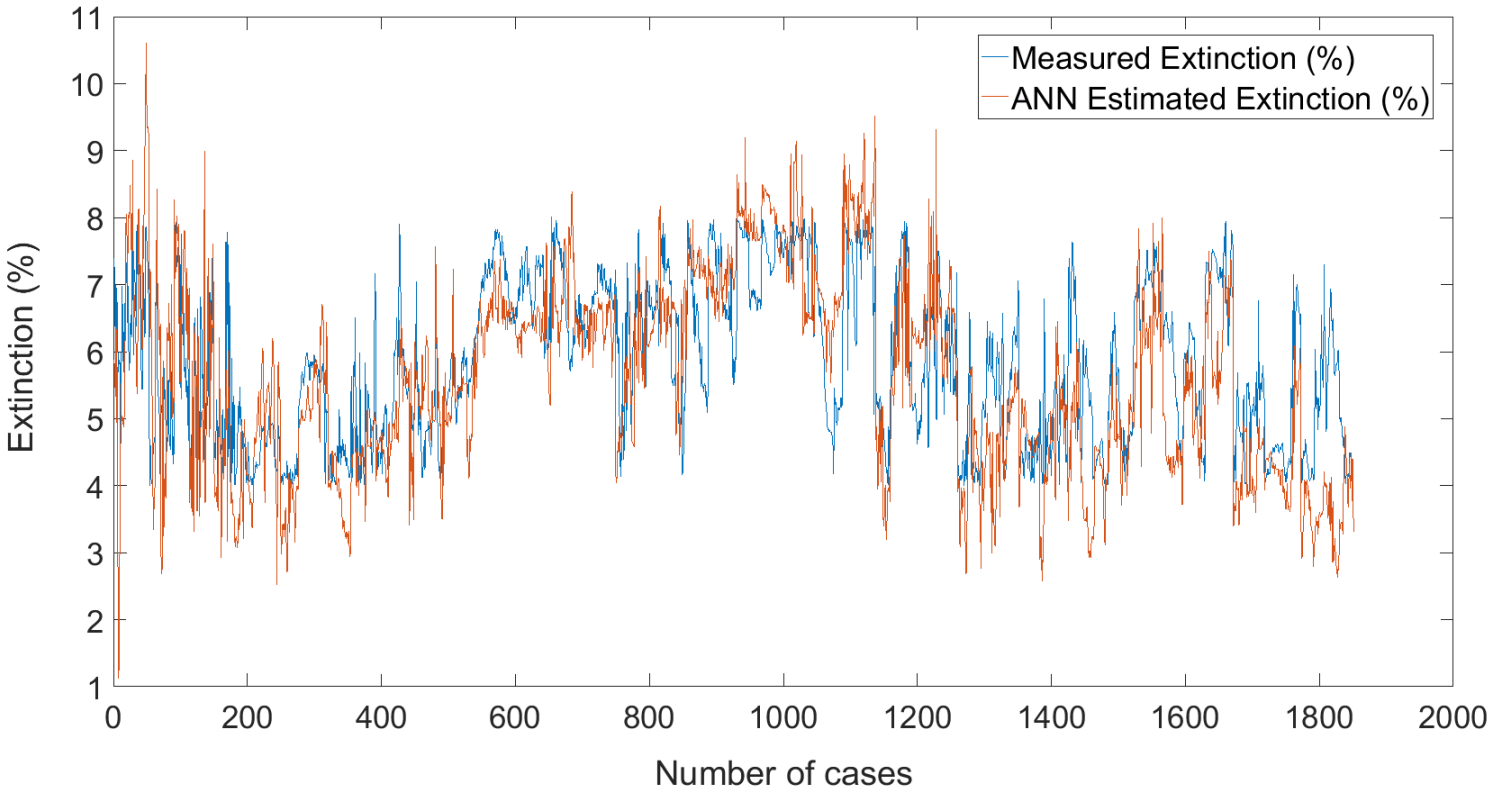

Figure 12: Scatter plot with the independent data set for testing and analyzing the ANN 2_2, where the Extinction is between 4 and 8%.

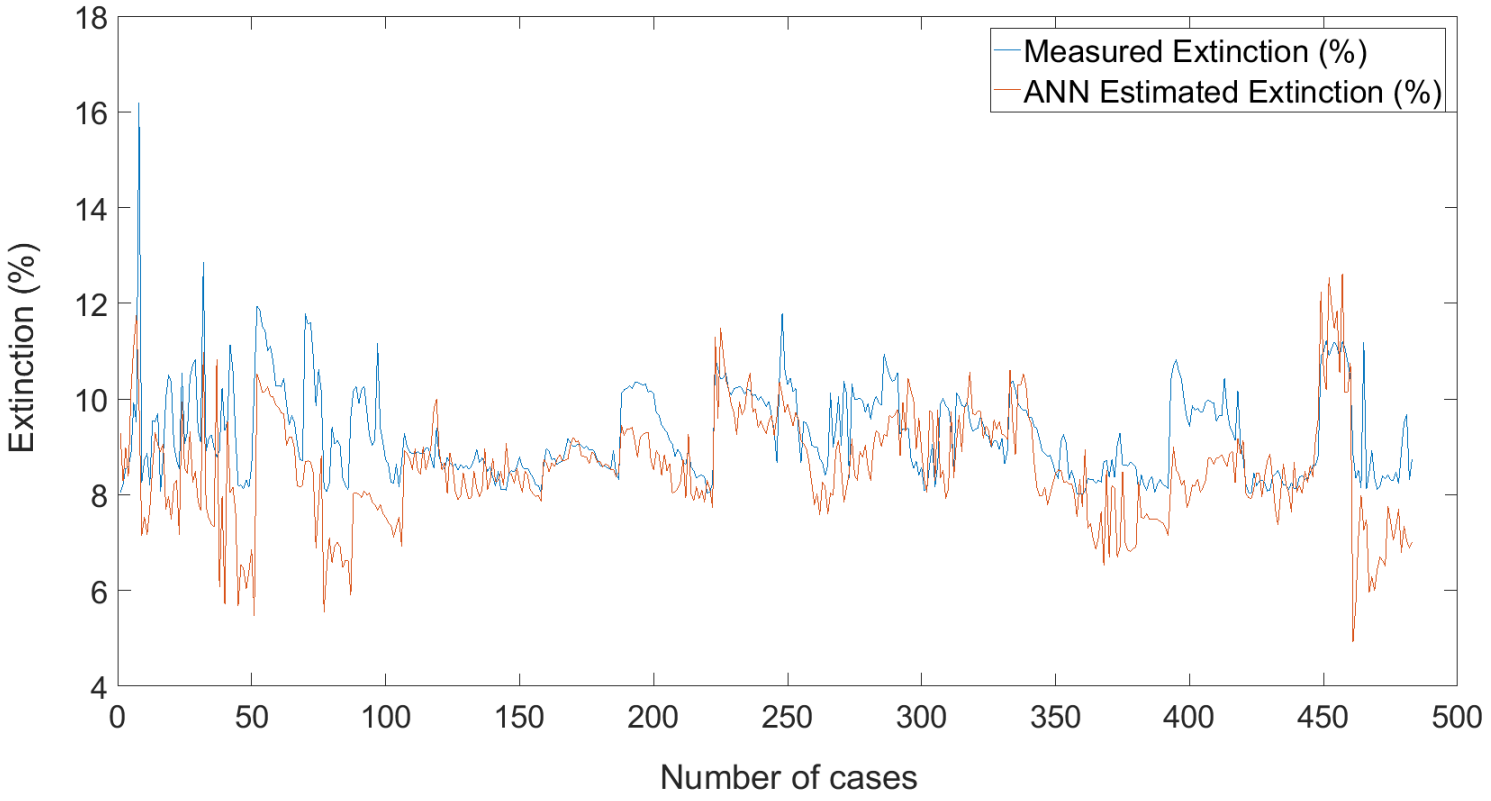

Figure 13: Scatter plot with the independent data set for testing and analyzing the ANN 2_2, where the Extinction is higher than 8%.